Journal of Environmental Chemical Engineering 9 (2021) 104966

Contents lists available at ScienceDirect

Journal of Environmental Chemical Engineering

journal homepage: www.elsevier.com/locate/jece

Fabrication of a metal-organic framework composite for removal of Aflatoxin B1 from water

Melvin S. Samuel [a], V.S. Kirankumar [b], E. Selvarajan [c,*]

[a] School of Environmental Science and Engineering, Indian Institute of Technology, Kharagpur 721302, West Bengal, India
[b] Nano & Green Analyical Lab, Department of Medicinal and Applied Chemistry, Kaohsiung Medical University, Kaohsiung City 807, Taiwan
[c] Department of Genetic Engineering, School of Bioengineering, SRM Institute of Science and Technology, Kattankulathur 603203, Chennai, Tamil Nadu, India

ARTICLE INFO

Editor: Dr. GL Dotto

Keywords:
Metal organic framework
Aflatoxin B1
Adsorption
Isotherms
Kinetics

ABSTRACT

The Aflatoxins are considered to be poisonous carcinogens as well as mutagens that are regularly found as a contaminant in the improperly stored commodities like the cottonseed, sesame seeds, cassava, chili peppers, sorghum, millet, peanuts, rice, sunflower seeds, sweetcorn, tree nuts, wheat, etc. The Aflatoxins are toxic metabolites that are capable of causing damages to the human as well as animal health by targeting the vital organs. Hence there is dire need to develop novel strategies for the development of the techniques for detoxification to produce contaminant free commodities. The Zinc terephthalate metal-organic framework [Zn(BDC)(DMF)]MOF catalyst prepared using the solvothermal method. In this study, Zn based MOF crystals funtionalized with amines were synthesized for the effective adsorption of the AFB1 and were characterized by the employment of SEM, FTIR, PXRD, BET and UV-DRS. In this study, the Zn(BDC)(DMF)MOF was employed as an adsorbent for the elimination of the Aflatoxin B1 (AFB1) from water. The maximum adsorption capacity of NH_2-Zn(BDC)(DMF) MOF composite for AFB1 was found to be 73.4 mg/g at 303 K and 6.0 pH conditions. The Langmuir and Freundlich isotherms were found to fit well in defining the adsorption performance as well as the kinetic data by the application of a pseudo-second-order model. The results reported that NH_2-Zn(BDC)(DMF)MOF can be employed as a suitable candidate capable of acting as an adsorbent for the removal AFB1.

1. Introduction

In the past few years, the contamination of cereal grains as well as the commonly employed animal feed by the mycotoxins has emerged as a very serious concern requiring consideration in the world. The estimated statistics report that about 25% of the food crops are prone to the contamination by the mycotoxins annually at a global scale [1,2]. The mycotoxins are the secondary metabolites that are secreted by the fungi under moist environments and are worldwide ubiquitous cause capable of polluting the environment. These secondary metabolites are found extensively as a contaminant within the feed as well as in the food products [3,4]. The consumption of the products contaminated by the mycotoxin like zearalenone (ZER), aflatoxin (AF), fumonisins, deoxynivalenol (DON) as well as ochratoxin harbors the potential to inflict severe damage as well as fatalities in the animals as well as the humans [5–8]. The Aflatoxins are a group of universally elaborated fungal toxin that occur naturally with a strong influence in the humans as well as animals causing serious biochemical as well as structural alterations in various organs like the lungs, liver, kidneys and the heart due to the mutagenicity and carcinogenicity possessed by them [2,4,9–11]. This type of mycotoxin is produced as a secondary metabolite by the *Aspergillus flavus* as well as *Aspergillus parasiticus* and the Aflatoxin B1 (AFB1) is considered to be the most toxic and carcinogenic toxin when compared to the other types of the Aflatoxins B2, G1 and G2. The consumption of food contaminated with the aflatoxin by the humans result in acute as well as chronic infections due to the mutagenic, hepatocarcinogenic and teratogenic property [12]. In the case of agricultural products as well as poultry production, the frequent contamination of the commodities with aflatoxins leads to wider extent decrease in the profitability of the particular sector. Currently the need to detoxify the contents that are contaminated with the aflatoxins to prevent the loss of health and profitability is the leading concern [13,14]. *A. flavus* has a world-wide distribution and normally occurs as a saprophyte in soil, water and on many kinds of decaying organic matter. *A. flavus* is the

* Corresponding author at: Department of Genetic Engineering, School of Bioengineering, SRM Institute of Science and Technology, Kattankulathur 603203, Chennai.
E-mail addresses: selvarae@srmist.edu.in, selrajan@gmail.com (E. Selvarajan).

https://doi.org/10.1016/j.jece.2020.104966
Received 15 October 2020; Received in revised form 9 December 2020; Accepted 17 December 2020
Available online 25 December 2020
2213-3437/

second most common species to be isolated from human infections. *A. flavus* produces AFB1 as a secondary metabolite that are released into the water environments [15,16].

The Metal organic framework (MOFs) is considered to be a progressively developing hybrid organic-inorganic supramolecular material that is constituted by clusters of metal ions and metal oxide that are joined together by a 3D structure using a organic linker [17–20]. These MOFs comprises high surface area as well as crystalline porous materials for their potential applications in the photoluminescence, heterogeneous catalysis, sensors, solar cells, hydrogen storage as well as in the CO_2 capture, drug delivery, adsorption as well as separation [21–26]. In the generalized concept, these MOFs can potentially be prepared from several combinations of the metallic counterparts as well as the ligands. In the MOFs, the metal ions act as the nodes, and the ligands play the role of bridges. Though the MOFs can be prepared by the employment of transition metal species, the non-noble metals are highly preferred instead owing to their availability. The MOFs synthesized employing iron, copper, zinc, cobalt, titanium, and zirconium have been already employed in the processes of hydrogen making, CO_2 capturing as well as in the gas storage, etc [12,27–34]. The researchers have reported that the ligands constituting the MOF can serve as probes for the production of light upon light irradiation and can potentially activate the metal nodes of the MOFs thereby representing a semiconductor like performance. This kind of a involved mechanism paves a path for several researchers to appropriately focus on the development of novel MOFs-based catalytic material with the ability to utilize the light for the purpose of degrading the pollutants that are present as contaminants in the water. Despite the development in the production of many types of MOFs, the application of them on the large scale potentially remains as a challenging task owing to their steadiness as well as degradation capacity in the efficiencies against selective contaminants that are abundant in the water [35–38]. The element Zinc is considered to be a vital mineral for the humans as they are involved in the regulation of growth, metabolic processes present within the abdominal microflora, blockade functions and it is also considered to be a potent antioxidant. Apart from this, the Zn complexes were found to have little or no harmfulness to the human cells at low amounts. In addition to this, Zn as a supplement in the animal diet results in improved growth performances, restriction of diarrhea, as well as in the enhancement of the duodenal microbiota.

In this study, synthesized Zn based MOF crystals were synthesized for the effective adsorption of the AFB1. The binding efficacy of adsorbent material were found to be greatly dependent upon their crystal structures, associated physical properties, and were also found to be dependent on the physicochemical properties of the aflatoxins [5], the modification of [Zn(BDC)(DMF)]MOF with amine can potentially lead to the enhancement of the efficacy for the purpose of binding AFB1. The objective of this study was to perform an investigation on the NH_2-[Zn(BDC)(DMF)]MOF as a new adsorbent for the elimination of AFB1 from the feedstock or water. This NH_2-[Zn(BDC)(DMF)]MOF serves as a porous template for the polymerization of dopamine. Dopamine consists of amine and catechol functional groups that not only adsorbs AFB1 but also provides a strong interaction to adhere the polymer onto the internal MOF structure. It also inhibits the dispersion of dopamine into water and, therefore it can be used several times as regenerative adsorbent.The effects of several parameters such as pH, initial AFB1 concentration, adsorbent dosage, contact time, and temperature were also investigated. Also, the adsorption behavior among the adsorbent and the AFB1 was assessed by adsorption isotherm and kinetic models. The NH_2-[Zn(BDC)(DMF)]MOF composite was found to harbor features excellent compliance, high adsorption capacity, better operational condition, negative secondary contamination generation, and explicit regeneration as a beneficial technique for the adsorption of AFB1.

2. Experimental section

2.1. Materials and Methods

2.1.1. Chemicals

A commercial $Zn(NO_3)_2.3\ H_2O$ (ACS reagent, 98% (Sigma-Aldrich), Benzene-1,4-dicarboxylic acid (BDC) with 96% purity (Sigma-Aldrich) and ethanol, potassium permanganate ($KMnO_4$), sulfuric acid (H_2SO_4), sodium nitrate ($NaNO_3$), Dopamine HCl, hydrogen peroxide (H_2O_2), hydrochloric acid (HCl) and aflatoxin B1 (AFB1) were purchased (Sigma-Aldrich).

2.1.2. Instrument details

Through scanning electron microscopy (SEM) using a Zeiss Auriga tool, the NH_2-[Zn(BDC)(DMF)]MOF was detected. Using PANalytical X'pert, the powder X-ray diffraction (PXRD) pattern of the synthesized MOFs were described.The spectra of Fourier transform infrared (FTIR) were reported as KBr pellets on a Nicolet NEXUS 470-FTIR spectrophotometer. The JASCO-V670 spectrophotometer is used for diffuse reflectance spectroscopy (DRS). N_2 adsorption isotherm was recorded using a Brunauer – Emmett – Teller (BET), ASAP 2010 micromeritic instrumental arrangement for evaluating the sample surface area and micropore.

2.2. Synthesis of [Zn(BDC)(DMF)]MOF composite

Preparation of adsorbent material. The [Zn(BDC)(DMF)]MOF catalyst was prepared using the solvothermal method. In this study, $Zn(NO_3)_2.3\ H_2O$ and Benzene-1,4-dicarboxylic acid (1:2 ratio) were added in 15 mL of N,N-dimethylformamide (DMF). The two chemicals were mixed and stirred until BDC was completely soluble. The miscible solution was transferred into a 100 mL Teflon-liner stainless autoclave. The autoclave was placed in the oven at 110 °C for 24 h. Then, the autoclave was allowed to cool down, and the white crystals were separated and washed with deionized water and ethanol. Further, the crystals were dried in an oven for 10 h.

2.2.1. Free Base Dopamine Synthesis

To 12 g of Dopamine HCl, 100 mL of anhydrous tetrahydrofuran (THF) and 100 mL of anhydrous methanol was added. 1.3 g of dry sodium hydride 95% was added slowly for20 minutes. The reaction mixture was carried out for 48 h in the presence of N_2 atmosphere. Subsequently, the accomplishment of the reaction, the obtain white powder was separated and kept under vacuum.

2.3. Synthesis of NH_2-[Zn(BDC)(DMF)]MOF composite

3 g of [Zn(BDC)(DMF)]MOF was activated at 110 °C under vacuum for 6 h in a 250 mL round bottom flask. After initiation, the sample was sealed under an inert atmosphere. In comparison to the as-prepared free base dopamine (6 g), 200 mL methanol solution, and 3 g activated[Zn(BDC)(DMF)]MOF was added and the reaction was carried out for 1 h, the white powder becomes dark brown suggesting the polymerisation reaction.The reaction sustained overnight at room temperature. After accomplishment, the obtained product was washed several times with methanol to remove the unbound amine group from [Zn(BDC)(DMF)]MOF. Subsequently, the product was dried under vacuum at room temperature.

All the adsorption experiments were performed at37°C temperature with a pH value of 6.0 adjusted by phosphate buffer. Adsorption experiments were carried out in a polypropylene glass container(30 mL). The stock solution of AFB1 (50 mg/L) was set by adding a required amount of mycotoxin into chromatographic grade methanol solution. The initial concentrations of working solutions varied from 5 − 50 mg/L for AFB1. In batch adsorption study, the prepared NH_2-Zn(BDC)(DMF) MOF was added into a 30 mL aliquot containing AFB1 at different initial

concentrations. The adsorption procedures were conducted at 37 °C, 120 rpm for 360 min. The supernatant was purified after the process using a 0.22 μm syringe filter, and 1 mL of the filtrate was taken by HPLC to measure the volume of AFB1. In triplicates, the tests were conducted and the mean average value was used to plot the graph.The equilibrium adsorption (q_e, mg/g) was determined using Eq. 1 [39–45]. RMSE; root-mean-square error Eqs. (2) and (3).

$$q_e = \frac{C_O - C_f}{M} \times V \tag{1}$$

$$R^2 = 1 - \frac{\sum_{n=1}^{n} (Y_{pred,.i} - y_{exp.i})^2}{\sum_{n=1}^{n} (Y_{pred,.i} - y_{exp.i})^2} \tag{2}$$

$$RMSE = \frac{1}{n-1} \sqrt{\sum_{n=1}^{n} (Y_{pred,.i} - y_{exp.i})^2} \tag{3}$$

Where C_o and C_f are the initial and equilibrium concentration of AFB1 respectively. V (L) is the volume of the solution, m(g) is the weight of the adsorbent and q_e(mg/g) is the adsorption capacity of the adsorbent.The HPLC study was carried out using mobile phase methanol: water isocratic (1:1, v / v) at 1 mL/min flow rate, 20 μL injection depth, and calculated by a UV detector at 360 nm respectively.The residual concentration after adsorption equilibrium and the adsorption amount q_e (mg/g) was calculated.

In order to describe the adsorption process, pseudo-first order and pseudo-second order models were employed. To determine the adsorption equilibrium Langmuir and Freundlich isotherm models were applied in our study. The Langmuir adsorption model can be expressed by Eqs. (4) and (5) as nonlinear and linear forms, respectively.

$$q_e = \frac{q_{\max} b C_{eq}}{1 + b C_{eq}} \tag{4}$$

$$\frac{1}{q_e} = \frac{1}{q_{\max}} + \frac{1}{q_{\max} b} \frac{1}{C_{eq}} \tag{5}$$

Where, q_e is the metal concentration adsorbed, C_{eq} is the remaining metal residual in solution, q_{max} is the maximum uptake with respect to adsorption sites saturation and b is the ratio of the adsorption/desorption rate.

The Langmuir isotherm can be described by a dimensionless equilibrium parameter R_L and determined by Eq. (6). Where R_L is known as separation factor and it is used for the applicability of adsorption process [45–51]. If $R_L < 1$, implies the favourable adsorption; $R_L = 0$ implies the adsorption process is irreversible; $R_L > 1$ implies the adsorption process is unfavourable and if $R_L = 1$ implies the adsorption process is linear.

$$R_L = \frac{1}{1 + K_L C_o} \tag{6}$$

The Freundlich adsorption isotherm is expressed in Eq. (7) and its linearized form is given in Eq. (8), here K_f and n are constants. Where C_{eq} is related to adsorption capacity and n is given as adsorption intensity.

$$q_e = K_f C_e^{\,1/n} \tag{7}$$

$$\log q_e = \log K_f + \frac{1}{n} \log C_e \tag{8}$$

Kinetic models are used for determining the adsorption mechanism in batch studies. The rate of AFB1 removal by NH_2-Zn(BDC)(DMF)MOF composite material was studied using three different kinetic models viz., pseudo-first order and pseudo-second order. The above mentioned kinetic models and their equations are given below:

$$\log (q_e - q_t) = \log q_{eq} - \frac{Kt}{2.303} \tag{9}$$

$$\frac{t}{q_t} = \frac{1}{K q_e^2} + \frac{1}{q_e} t \tag{10}$$

Where, q_e is the amount of adsorbate (mg) adsorbed per unit mass (g) of adsorbent at equilibrium, q_t is the amount of adsorbate (mg) adsorbed per unit mass (g) of adsorbent at time t, K1 is the rate constant (1/min) for pseudo first order reaction, K_2 is the rate constant (g/mg/min) for pseudo second order reaction, R_{id} is the intra-particle diffusion rate constant (mg/g $min^{-0.5}$).

3. Results and discussion

3.1. Characterization of MOF composite

The FTIR was recorded for NH_2-Zn(BDC)(DMF)MOF and it is shown in Fig. 1. The NH_2-Zn(BDC)(DMF)MOF displays a sign at 3606 cm^{-1} and 3170 cm^{-1} (-OH peak); 3170 cm^{-1} (C-H stretch); 1700 cm^{-1} (C=O stretch); 1577 cm^{-1} (–CO_2 stretch); 1369 cm^{-1} agrees to carboxylate collections. The peaks at 1145 cm^{-1}, 1102 cm^{-1}, and 1015 cm^{-1} responsible for C-C stretching. polydopamine represented by the presence of three sharp peaks, i.e., aromatic C-C stretching at 1490 cm^{-1}, NH_2 in-plane bending at 1490 cm^{-1}, and C-O-H symmetric bending at 1266 cm^{-1} could be detected. The presence of these bands represents the presence of polydopamine.The crystallographic structure of the products was determined by PXRD. The PXRD of synthesized NH_2-Zn(BDC)(DMF)MOF is shown in Fig. 2. The crystal phase of NH_2-Zn(BDC)(DMF)MOF was recorded over the diffraction angle (2Θ) of 5 – 50°. The PXRPD pattern of synthesized NH_2-Zn(BDC)(DMF)MOF, displayed distinctive points at 2Θ = 10.2°, 12.5°, 14.2°, 24.3°, 27.06°, 31.17°, and 42.82°. The well-defined diffraction peaks revealed the high crystallinity of the Zn(BDC)(DMF)MOF. The Zn(BDC)(DMF)MOF and NH_2-Zn(BDC)(DMF)MOF exhibit the same diffraction pattern, indicating that the crystal phase structure is retained after amine functionalization.

The size and shape of NH_2-Zn(BDC)(DMF)MOF was observed by scanning electron microscopy (SEM). As shown in Fig. 3a. Zn(BDC)(DMF)MOF catalyst showed a distinct, steady, and brick-shaped assembly. Whereas, NH_2-Zn(BDC)(DMF)MOF catalyst exhibited spindle-shaped morphology and needle-shaped, indicating the attachment of amine molecule onto Zn(BDC)(DMF)MOF (Fig. 3b). The UV–vis DRS analysis for NH_2-Zn(BDC)(DMF)MOF was recorded in the span of 200 – 800 nm and the results are depicted in Fig. 4a.The optical bandgap of the result is calculated from the Tauc relation equation [52]. The Kubelka-Munk theory F(R) is used for evaluating the optical reflectance property using the Eq. (11):

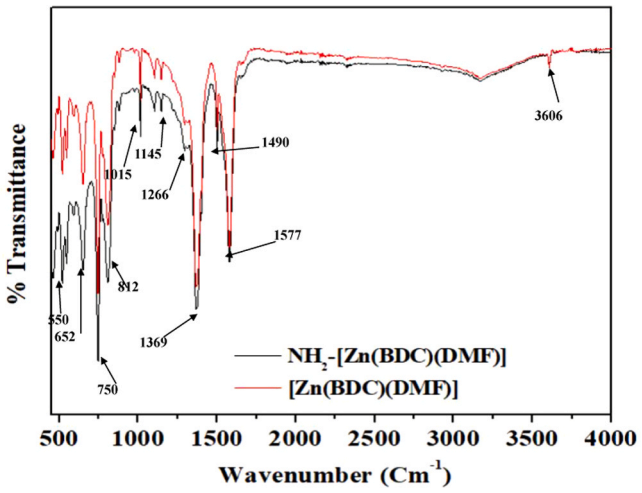

Fig. 1. FT-IR spectra of [Zn(BDC)(DMF)]MOF and NH_2-[Zn(BDC)(DMF)]MOF.

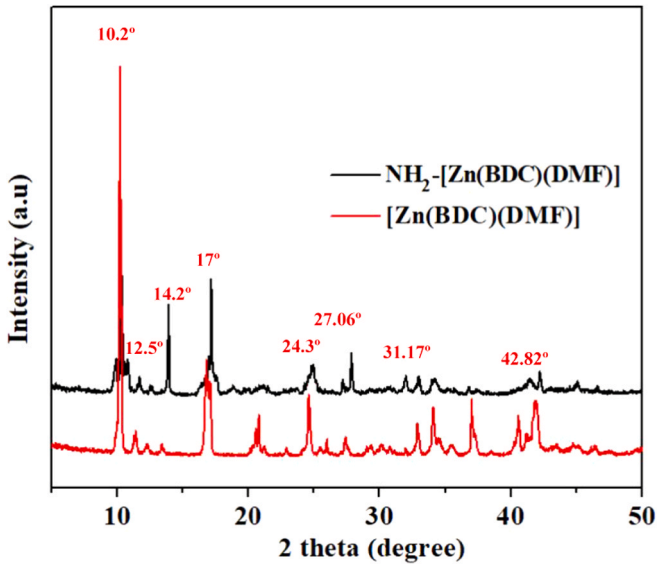

Fig. 2. PXRD pattern of [Zn(BDC)(DMF)]MOF and NH_2-[Zn(BDC)(DMF)]MOF.

$$\alpha = F(R) = \frac{(1-R)^2}{2R} \quad (11)$$

Where F (R) is Kubelka–Munk theory, R is a reflectance of the compound, and α is an absorption coefficient. Consequently, the Tauc plot relation Eq. (12) develops:

$$F(R)\,h\nu = A\left(h\nu - E_g\right)^2 \quad (12)$$

Where, h is a Planck's constant, E_g is an optical band gap energy, ν is a photon frequency, and A is a constant. The plot $(F(R)\ h\nu)^2$ versushν is shown in Fig. 4b. The bandgap of NH_2-Zn(BDC)(DMF)MOF material is 3.80 eV. The bandgap of NH_2-Zn(BDC)(DMF)MOF is like the outcomes depicted by Herrera et al. [53]. Nitrogen adsorption-desorption isotherms have determined the precise surface area and porous composition of NH_2-Zn(BDC)(DMF)MOF. The NH_2-[Zn(BDC)(DMF)]MOF catalyst showed the pore volume (P_{vol} - 0.0924 cm^3/g), pore size (P_{size} – 31.173 Å) and a precise area of 545.5 m^2/g for the NH_2-Zn(BDC)(DMF) MOF. The NH_2-Zn(BDC)(DMF)MOF showed a higher explicit area and large porosity. No leaching of Zn ions was observed per ICP-MS, which shows a no Zn concentration in the detectable range limit (<1 ppb). Also, after long-term soaking, there is no apparent trace of polydopamine found in the water samples.

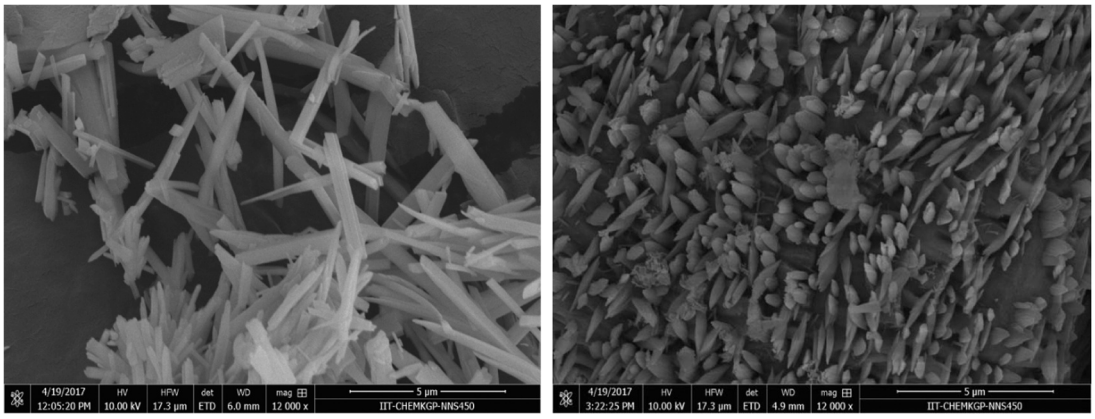

Fig. 3. SEM image of (a) Zn(BDC)(DMF)MOF and (b) NH_2-[Zn(BDC)(DMF)]MOF.

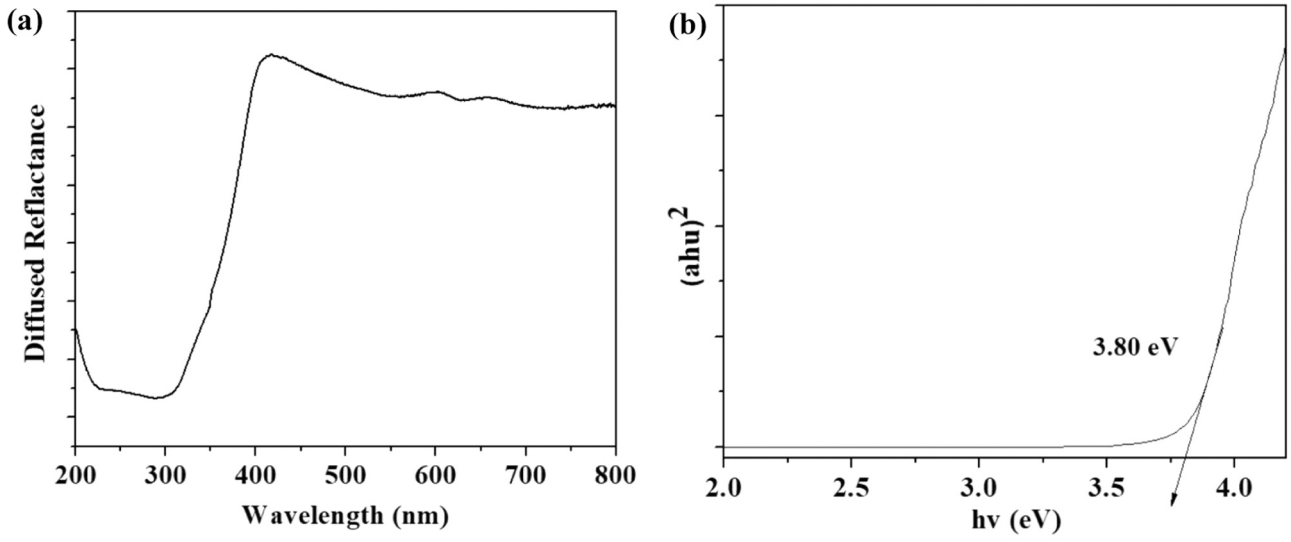

Fig. 4. Optical properties of NH_2-[Zn(BDC)(DMF)]MOF sample: (a) Diffused reflectance spectra (b) Tauc's plot.

3.2. Adsorption equilibrium data

The adsorption behavior of NH_2-Zn(BDC)(DMF)MOF validated by AFB1 removal percentage. Fig. 5 shows that the removal of AFB1 decreases with increase in AFB1 concentration, whereas the adsorption capacity increases with increase in AFB1 concentration, this is probably due to the availability of a large number of binding sites available for AFB1 adsorption onto NH_2-Zn(BDC)(DMF)MOF (Fig. 5). The results validate that the removal of AFB1 is highly concentration dependant. It is to be noted that at lower concentrations of AFB1, the AFB1 present in the solution are comparatively lesser as compared to the number of available sites on the NH_2-Zn(BDC)(DMF)MOF. Whereas at higher concentration of AFB1 in the solution, the available sites for the adsorption becomes lesser, thereby the removal percentage of AFB1 depends on initial concentration. The effect of contact time on the adsorption of AFB1 onto NH_2-Zn(BDC)(DMF)MOF was depicted in Fig. 6a. As shown in Fig. 6a, the 30% AFB1 adsorbed within 60 min, whereas 90% adsorption occurs at 360 min, thereafter the adsorption reaches equilibrium. The effect of pH on the adsorption ofAFB1onto NH_2-Zn(BDC)(DMF)MOF was depicted in Fig. 6b. There occurs a slight decrease in the adsorption of AFB1 was observed when the pH was below 6.0, suggesting that slight desorption of AFB1might have happened when the pH value is acidic. The findings show that NH_2-Zn (BDC)(DMF)MOF displays adsorption of AFB1 in all pH ranges.The point of zero charge (pHpzc) of NH_2-Zn(BDC)(DMF)MOF adsorbent is 6.2. The point of zero charge is the pH at which the surface of your NH_2-Zn(BDC) (DMF)MOF adsorbent neutral. If the solution pH is less than pHzpc, the NH_2-Zn(BDC)(DMF)MOF adsorbent is positively charged. Otherwise the surface is negatively charged [54]. The NH_2-Zn(BDC)(DMF)MOF acquire a positive surface charge at pH 6.0 leading to a higher MOF uptake capacity. All adsorption studies were carried out at pH 6.0. The as-synthesized NH_2-Zn(BDC)(DMF)MOF showed a zeta potential of 3.15 mV. For in vitro adsorption of AFB1 by IMTX-hydrated sodium calcium aluminosilicate, the binding potential for AFB1 did not improve as the pH increased from 3 to 9 [55]. Similar findings were obtained by Ledoux et al. [56]. In this study, pH 6.0 was found to be suitable for AFB1by NH_2-Zn(BDC)(DMF)MOF.Fig. 6c displays the AFB1 adsorption into NH_2-Zn(BDC)(DMF)MOF at varying temperatures. As the solution temperature increased, the volume of AFB1 adsorption decreased, suggesting that the lower temperature led to the better adsorption operation.Higher the temperature, the randomness of the molecules is greater. It will then be impossible to get adsorbed on the surface of the NH_2-Zn (BDC)(DMF)MOF adsorbent by the AFB1. Therefore, adsorption decreases as the temperature of the adsorbate increases [56]. To reduce the adsorbent cost, the adsorbent material has to be regenerated for multiple cycles.

Regeneration of the NH_2-Zn(BDC)(DMF)MOF adsorbent was investigated using reagents such as EDTA(ethylenediaminetetraacetic acid) for the desorption of AFB1. For this experiment, required amount of NH_2-Zn(BDC)(DMF)MOF adsorbent was added to AFB1 containing solution. After the incubation time, the samples were filtered, dried, and weighed. The AFB1concentrations in the aqueous media were analyzed and qe (mg/g) was calculated. The samples were added to 0.001 M solutions of EDTA (2%HNO_3) allowed to shake at 100 rpm for 3 h. The samples were filtered,washed with methanol, dried and weighed. The regenerated NH_2-Zn(BDC)(DMF)MOF adsorbent were then added to AFB1 stock solution. This procedure was repeated 4 more times to obtain the capacity qe (mg/g) for each of the 5 cycles. Regeneration was performed using methanol. In comparison, to the 1st cycle, the NH_2-Zn (BDC)(DMF)MOF composite showed decreased adsorption performance by less than 11% in the fifth cycle. The NH_2-Zn(BDC)(DMF)MOF material holds great potential in the mycotoxin treatment of contaminants present in the water. This NH_2-Zn(BDC)(DMF)MOF can be restored and recycled, and able to absorb more than 89% of AFB1 even after five cycles shown in Fig. 6d. There is a slow reduction in the adsorption process of AFB1, which might be owing to the loss of porosity in the NH_2-Zn(BDC)(DMF)MOF. After the adsorption, the effluent was analysed for secondary contamination/leaching from NH_2-Zn(BDC)(DMF) MOF. No secondary contamination/leaching was observed. Similarly, adsorption studies was conducted in the presence of natural organic matter (NOM), there occurs no significant decrease in the AFB1 adsorption.

The adsorbent NH_2-Zn(BDC)(DMF)MOF's equilibrium adsorption increased dramatically with the rise of the initial AFB1 concentration. Different theoretical models analyze the adsorption isotherm data to estimate the adsorbent's saturation point, the adsorbent's surface properties and the adsorption mode.To suit the adsorption results, the Langmuir and Freundlich isothermal adsorption models were used. Fig. 7(a, b) displays the fitting line of the isothermal adsorption models and Table 1 lists the related parameters and correlation coefficient (R^2). NH_2-Zn(BDC)(DMF)MOF adsorption data suits both Langmuir and Freundlich models, as both R^2 models are 0.99. The models of isotherms show that NH_2-Zn(BDC)(DMF)MOF is consistent with the models of Langmuir and Freundlich and verifies monolayer and multilayer adsorption over the surface of NH_2-Zn(BDC)(DMF)MOF. Table 2 showed a comparison of the adsorption capacities of different adsorbents for

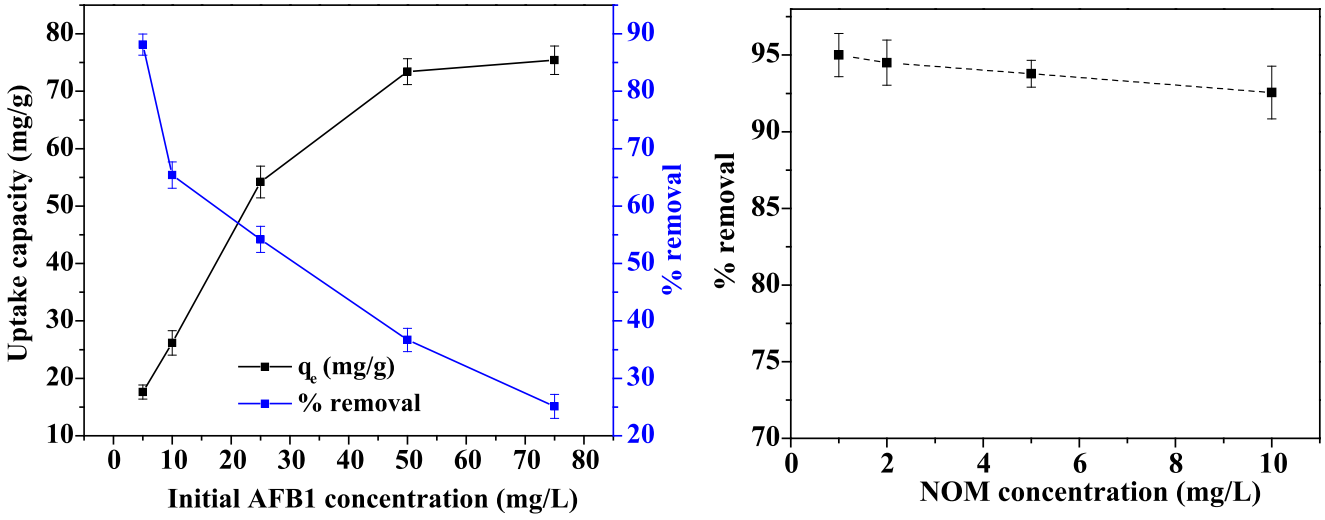

Fig. 5. (a) Batch adsorption performance and kinetics analysis. AFB1 adsorption uptake capacity and removal percentage of NH_2-[Zn(BDC)(DMF)]MOF with different initial AFB1 concentrations. (b) Removal efficiency of AFB1 in presence of NOM (0 – 10 mg L^{-1}/).

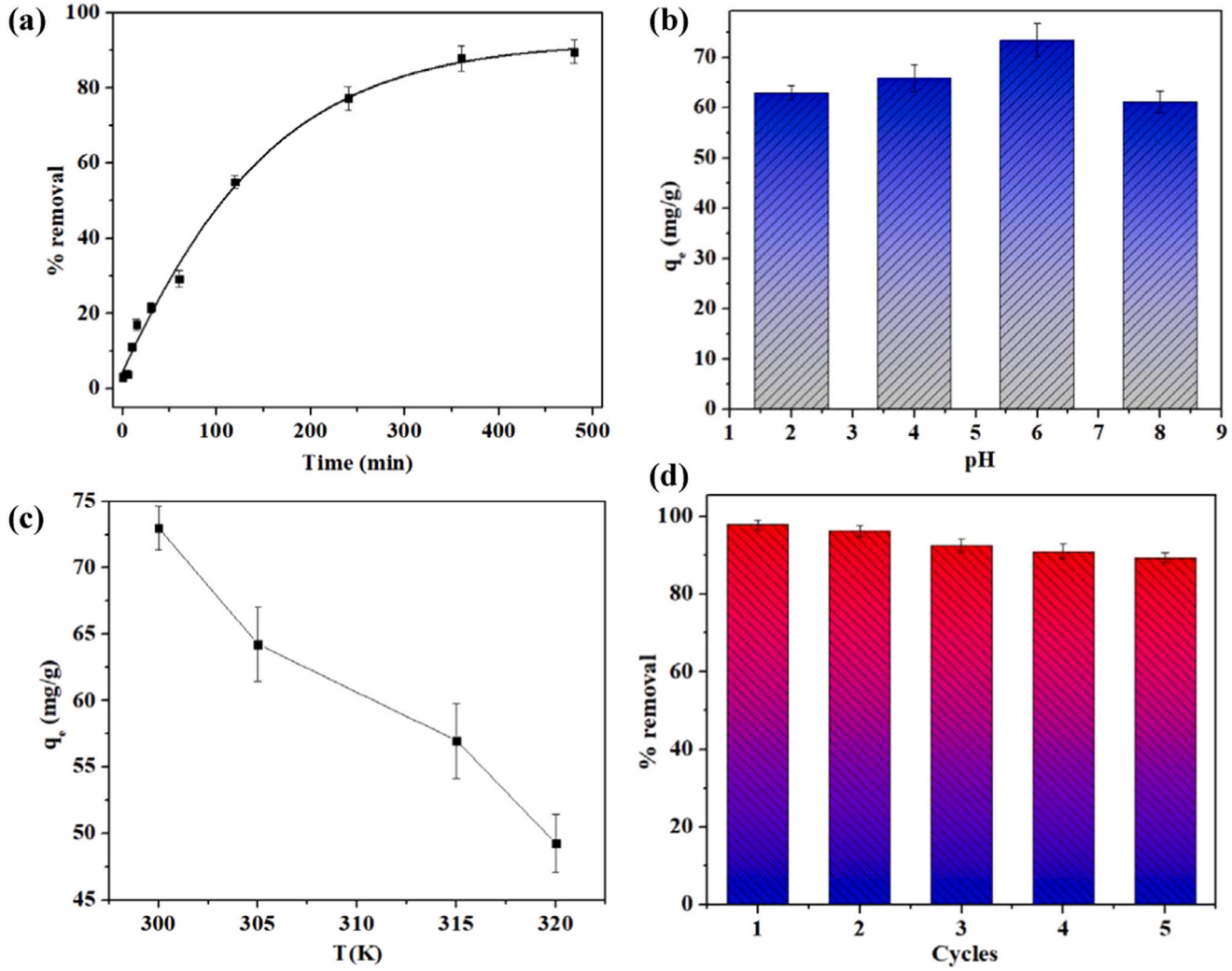

Fig. 6. Batch adsorption performance and kinetics analysis. (a) Effect of initial AFB1 concentration, (b) pH, (c) temperature, (d) recycle times of NH_2-Zn(BDC)(DMF) MOF (d) on AFB1 removal (AFB1 solution of C_0 = 50 mg/L; T = 300 K; dosage = 0.25 g/L; V = 30 mL; pH = 6.0).

AFB1. For the analysis of the adsorption mechanism, pseudo-first-order and pseudo-second-order kinetic models were used and key parameters for adsorption of AFB1 to NH_2-Zn(BDC)(DMF)MOF were given in Table 3. The values of root mean square error (RMSE) values are presented in Table 3 in order to assess the fitness of the kinetic models. For the pseudo-second-order kinetic model, the correlation coefficients (R^2) were in the range of 0.998 − 0.999, higher than pseudo-first-order kinetic model (Fig. 7c, d). Mechanism of the AFB1 adsorption to NH_2-Zn (BDC)(DMF)MOF. The chemical interface could occur between AFB1 to NH_2-Zn(BDC)(DMF)MOF in three different ways. The metal sites in NH_2-Zn(BDC)(DMF)MOF catalyst are partly positive charge [32,33], the Zn metal group can interact with AFB1 through the formation of chelation complexes of these ions with dicarbonyl system of AFB1 and ion–dipole interactions between Zn cation cations and carbonyl groups of AFB1. The BET analysis for NH_2-Zn(BDC)(DMF)MOF before and after AFB1 adsorption was done. After adsorption, the pore volume of NH_2-Zn(BDC) (DMF)MOF decreased from 0.09246 to 0.016 cm^3/g and pore size was changed from 31.174 to 7.395 Å.

The structure/assembly of AFB1is shown in the scheme. 1, which encompasses a tetrahydrocyclopenta[*c*]furo[3′,2′:4,5]furo[2,3-*h*]chromene skeleton with oxygen functionality at positions 1, 4 and 11. The coordinatively unsaturated sites (CUS) in NH_2-Zn(BDC)(DMF)MOF engaged by water in aqueous solution,the electrostatic interface between [Zn(BDC)(DMF)]MOF catalyst and AFB1can relocate water particles [34]. Thus, this carbonyl site of the AFB1 can be haggard towards the positively charged metal sites of NH_2-Zn(BDC)(DMF)MOF, resulting in adsorption of AFB1 to NH_2-Zn(BDC)(DMF)MOF as the route (a) of the scheme. 1. The NH_2-Zn(BDC)(DMF)MOF comprising of benzene carboxylic groups and amine modification can attract molecules containing benzene groups via the π– π stacking interaction [36]. Thus, AFB1 containing benzene ring is more likely to be drawn toward NH_2-Zn (BDC)(DMF)MOF via π– π stacking interaction as shown in the scheme. 1.

4. Conclusion

In this study, NH_2-Zn(BDC)(DMF)MOF was employed for the adsorptive elimination of the AFB1 that was prevalent in the water. The synthesized NH_2-Zn(BDC)(DMF)MOF consisted of two Zn(II) metal ions that were connected by four terephthalic acids resulting in the formation of $Zn_2(COO)_4$ paddle-wheel subordinate construction units. The kinetic data was found to be close-fitting to the pseudo-second-order. Similarly, the adsorption isotherm was found to be well fitted to the Langmuir and Freundlich isotherm models, suggesting that AFB1 is sorbed as a monolayer coverage on the functional group sites of NH_2-Zn(BDC) (DMF)MOF. Furthermore, it was reported from the study that NH_2-Zn (BDC)(DMF)MOF possess excellent regeneration ability as well as high adsorption potential even after processing for five cycles. Therefore,

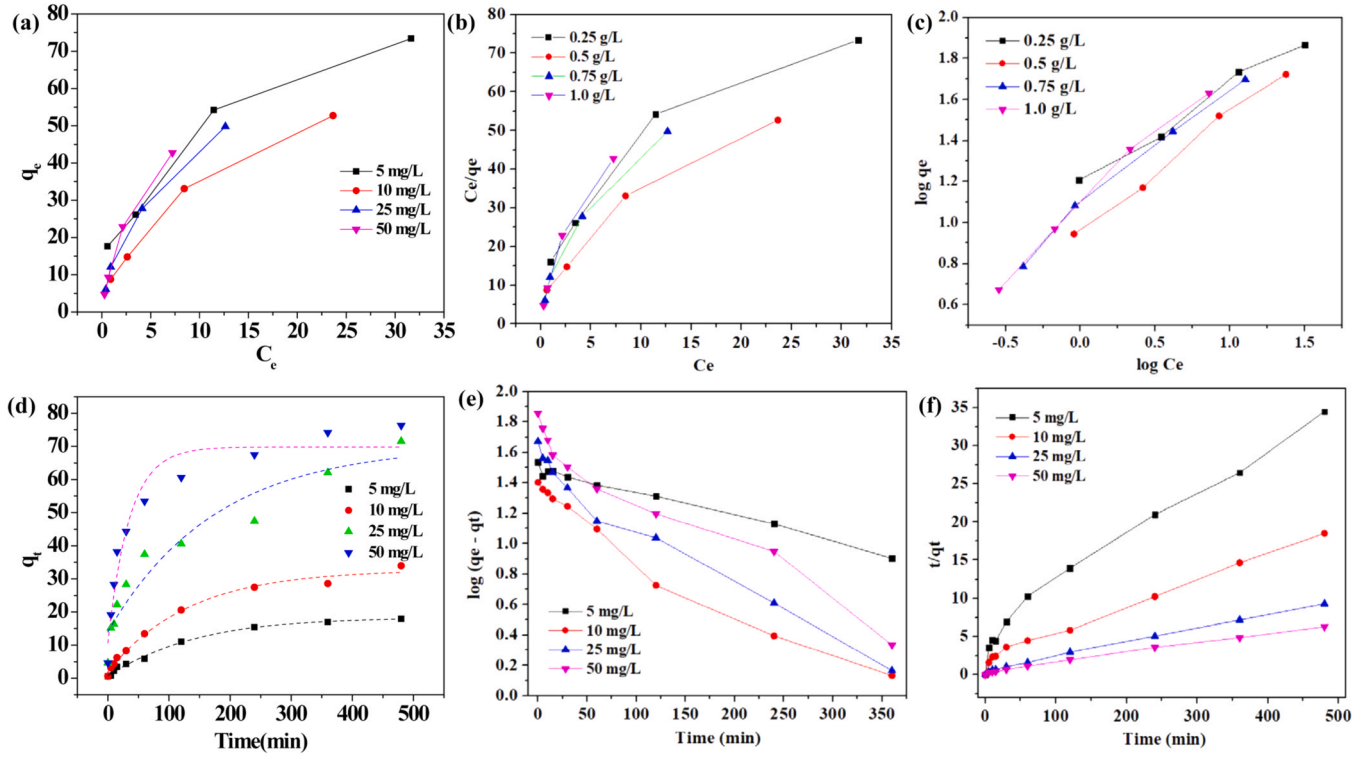

Fig. 7. The fitting lines of Non-linear Langmuir (a) and Linear Langmuir model (b), Freundlich model (c), Kinetic plot (d), pseudo-first-order model (e), pseudo-second-order model (f).

Table 1
Equilibrium isotherm parameters for the AFB1 adsorption on $NH_2Zn(BDC)(DMF)MOF$.

Isotherm models	Parameters	**0.25 g/L**	**0.50 g/L**	**0.75 g/L**	**1.0 g/L**
Experimental	q_e(mg/g)	**75.4**	**52.70**	**49.80**	**42.76**
Langmuir	q_{max} (mg/g)	73.45	57.51	46.22	45.78
	K_L (L/mg)	0.202	0.110	0.221	0.255
	R^2	0.9926	0.9958	0.9901	0.9972
Freundlich	K_f (mg/g)	19.76	9.15	11.42	11.93
	N	2.66	1.77	1.66	1.45
	R^2	0.9610	0.998	0.9902	0.9803

Table 2
Kinetics parameters for the adsorption of Cr(VI) by GO-FH bio-nanocomposite material based on different concentrations.

Concentration (mgL^{-1})	**5**	**10**	**25**	**50**
Experimental q_e (mg g^{-1})	16.2	28.5	82.05	77.51
Pseudo- first order				
K_1 (min^{-1})	5.98×10^{-3}	7.13×10^{-3}	8.06×10^{-3}	8.29×10^{-3}
q_e (mg/g)	35.44	20.30	32.71	49.78
R^2	0.9803	0.9817	0.9888	0.9968
RMSE	0.6721	1.554	1.109	1.105
Pseudo– second order				
K_2 (min^{-1})	0.014	0.021	0.049	0.052
q_e (mg/g)	15.64	28.01	52.19	74.51
R^2	0.9685	0.9874	0.9966	0.9958
RMSE	1.866	2.1791	3.024	1.341

these NH_2-Zn(BDC)(DMF)MOF can be employed potentially for the process of mycotoxin separation. In view of the suitable adsorption rate and adsorption capacity, the possibility of NH_2-Zn(BDC)(DMF)MOF as a exceedingly effectual AFB1 sorbent was exhibited thereby proving that they can act as excellent candidates for the detoxification of mycotoxin polluted environments.

Table 3
Comparison of the adsorption performance of different adsorbents for AFB1.

Adsorbents	Temperature (°C)	pH	q_{max} (mg/g)	References
OTAB-Mt	37	3.5	20.08	[1]
Octylphenol polyoxyethylene ether modified montmorillonite	37	3.5	2.72	[2]
Aluminum-iron-pillared montmorillonite	37	2.0	0.67	[3]
Glucomannan-modified hydrated sodium calcium aluminosilicate	37	7.0	1.74	[4]
NYSEP	37	3.5	4.53	[5]
Rectorite	37	3.5	8.05	[6]
1.5NZMt	37	3.5	49.26	[7]
FNHMS-0.4	37	7.0	27.34	[8]
NH_2-Zn(BDC)(DMF)MOF composite	27	7.0	73.4	This study

CRediT authorship contribution statement

Melvin S. Samuel designed the study and reviewed the paper; Melvin S. Samuel and V.S. Kirankumar conducted experiment and made primary draft; E. Selvarajan designed experiment supervised, reviewed, data analysis and made final version.

Declaration of Competing Interest

The authors declare that they have no known competing financial interests or personal relationships that could have appeared to influence the work reported in this paper.

Acknowledgment

Dr. Melvin Samuel. S is deeply thankful to the School of

Environmental Science and Engineering, Indian Institute of Technology Kharagpur for the fellowship.

Appendix A. Supporting information

Supplementary data associated with this article can be found in the online version at doi:10.1016/j.jece.2020.104966.

References

[1] M. Eskola, G. Kos, C.T. Elliott, J. Hajšlová, S. Mayar, R. Krska, Worldwide contamination of food-crops with mycotoxins: Validity of the widely cited 'FAO estimate' of 25%, Crit. Rev. Food Sci. Nutr. 60 (2020) 2773–2789.

[2] M.S. Samuel, A. Sivaramakrishna, A. Mehta, Degradation and detoxification of aflatoxin B1 by Pseudomonas putida, Int. Biodeterior. Biodegrad. 86 (2014) 202–209.

[3] C.O. Parker, I.E. Tothill, Development of an electrochemical immunosensor for aflatoxin M1 in milk with focus on matrix interference, Biosens. Bioelectron. 24 (2009) 2452–2457, https://doi.org/10.1016/j.bios.2008.12.021.

[4] M. Farzaneh, Z.Q. Shi, A. Ghassempour, N. Sedaghat, M. Ahmadzadeh, M. Mirabolfathy, M. Javan-Nikkhah, Aflatoxin B1 degradation by Bacillus subtilis UTBSP1 isolated from pistachio nuts of Iran, Food Control 23 (2012) 100–106, https://doi.org/10.1016/j.foodcont.2011.06.018.

[5] J. Varga, Z. Péteri, K. Tábori, J. Téren, C. Vágvölgyi, Degradation of ochratoxin A and other mycotoxins by Rhizopus isolates, Int. J. Food Microbiol. 99 (2005) 321–328, https://doi.org/10.1016/j.ijfoodmicro.2004.10.034.

[6] B.D. Malhotra, S. Srivastava, M.A. Ali, C. Singh, Nanomaterial-based biosensors for food toxin detection, Appl. Biochem. Biotechnol. 174 (2014) 880–896.

[7] M. Ngundi, L. Shriver-Lake, M.H. Moore, F.S. Ligler, C.R. Taitt, Multiplexed detection of mycotoxins in foods with a regenerable array, J. Food Prot. 69 (2006) 3047–3051.

[8] M.S. Samuel, Aflatoxin and public health – a population study, Int. J. Pharm. Sci. Heal. Care. 2 (2012) 52–61.

[9] J.F. Alberts, W.C.A. Gelderblom, A. Botha, W.H. van Zyl, Degradation of aflatoxin B1 by fungal laccase enzymes, Int. J. Food Microbiol. 135 (2009) 47–52, https://doi.org/10.1016/j.ijfoodmicro.2009.07.022.

[10] L. Yu, Y. Zhang, C. Hu, H. Wu, Y. Yang, C. Huang, N. Jia, Highly sensitive electrochemical impedance spectroscopy immunosensor for the detection of AFB1 in olive oil, Food Chem. 176 (2015) 22–26, https://doi.org/10.1016/j.foodchem.2014.12.030.

[11] O.D. Teniola, P.A. Addo, I.M. Brost, P. Färber, K.D. Jany, J.F. Alberts, W.H. Van Zyl, P.S. Steyn, W.H. Holzapfel, Degradation of aflatoxin B1 by cell-free extracts of rhodococcus erythropolis and mycobacterium fluoranthenivorans sp. nov. DSM44556T, Int. J. Food Microbiol. 105 (2005) 111–117, https://doi.org/10.1016/j.ijfoodmicro.2005.05.004.

[12] I. Karuppusamy, M.S. Samuel, E. Selvarajan, S. Shanmugam, P. Sahaya Murphin Kumar, K. Brindhadevi, A. Pugazhendhi, Ultrasound-assisted synthesis of mixed calcium magnesium oxide (CaMgO2) nanoflakes for photocatalytic degradation of Methylene blue, J. Colloid Interface Sci. 584 (2021) 770–778, https://doi.org/10.1016/j.jcis.2020.09.112.

[13] M.S. Samuel, Approaches in determining Aflatoxin B1 in food materials using a range of analytical methods. Int. J. Adv. Res. 1 (2013) 56–59.

[14] S. Needhidasan, M.S. Samuel, Existing methods for detoxification of aflatoxin, Int. J. Od. Adv. Res. 1 (2013) 43–46.

[15] N. Banu, B. Malaikumar, S. Pavithra, Enumeration of Terrestrial mycobiota and aflatoxin in drinking water, Asian J. Microbiol. Biotechnol. Environ. Sci. 18 (2016) 211–221.

[16] M. Samuel, Aflatoxin B 1 occurance, biosynthesis and its degradation, J. Pure Appl. Microbiol. 7 (2013) 0–7.

[17] M.S. Samuel, J. Bhattacharya, C. Parthiban, G. Viswanathan, N.D. Pradeep Singh, Ultrasound-assisted synthesis of metal organic framework for the photocatalytic reduction of 4-nitrophenol under direct sunlight, Ultrason. Sonochem. 49 (2018) 215–221.

[18] M.S. Samuel, V. Subramaniyan, J. Bhattacharya, C. Parthiban, S. Chand, N.D. P. Singh, A GO-CS@MOF [Zn(BDC)(DMF)] material for the adsorption of chromium(VI) ions from aqueous solution, Compos. Part B Eng. 152 (2018) 116–125, https://doi.org/10.1016/j.compositesb.2018.06.034.

[19] M.H. Dehghani, K. Yetilmezsoy, M. Salari, Z. Heidarinejad, M. Yousefi, M. Sillanpää, Adsorptive removal of cobalt(II) from aqueous solutions using multi-walled carbon nanotubes and γ-alumina as novel adsorbents: modelling and optimization based on response surface methodology and artificial neural network, J. Mol. Liq. 299 (2020), 112154.

[20] A. Dehghan, A.A. Mohammadi, M. Yousefi, A.A. Najafpoor, M. Shams, S. Rezania, Enhanced kinetic removal of ciprofloxacin onto metal-organic frameworks by sonication, process optimization and metal leaching study, Nanomaterials 9 (2019), 1422.

[21] Y. Hosogi, H. Kato, A. Kudo, Photocatalytic activities of layered titanates and niobates ion-exchanged with sn2+under visible light irradiation, J. Phys. Chem. C. 112 (2008) 17678–17682.

[22] A. Rezk, R. Al-Dadah, S. Mahmoud, A. Elsayed, Characterisation of metal organic frameworks for adsorption cooling, Int. J. Heat. Mass Transf. 55 (2012) 7366–7374.

[23] F. Bella, R. Bongiovanni, R.S. Kumar, M.A. Kulandainathan, A.M. Stephan, Light cured networks containing metal organic frameworks as efficient and durable polymer electrolytes for dye-sensitized solar cells, J. Mater. Chem. A. 1 (2013) 9033–9036.

[24] C. Gerbaldi, J.R. Nair, M.A. Kulandainathan, R.S. Kumar, C. Ferrara, P. Mustarelli, A.M. Stephan, Innovative high performing metal organic framework (MOF)-laden nanocomposite polymer electrolytes for all-solid-state lithium batteries, J. Mater. Chem. A. 2 (2014) 9948–9954.

[25] C. Parthiban, M. Pavithra, L.V.K. Reddy, D. Sen, M.S. Samuel, N.D.P. Singh, Tetraphenylethylene conjugatedp-hydroxyphenacyl: fluorescent organic nanoparticles for the release of hydrogen sulfide under visible light with real-time cellular imaging, Org. Biomol. Chem. 16 (2018) 7903–7909, https://doi.org/10.1039/c8ob01629a.

[26] S. Datta, K.N. Rajnish, M.S. Samuel, A. Pugazlendhi, E. Selvarajan, Metagenomic applications in microbial diversity, bioremediation, pollution monitoring, enzyme and drug discovery. A review, Environ. Chem. Lett. 18 (2020) 1229–1241.

[27] M. Zhao, S. Ou, C.-D. Wu, Porous metal?organic frameworks for heterogeneous biomimetic catalysis, Acc. Chem. Res. 47 (2014) 1199–1207.

[28] S.-H. Huo, X.-P. Yan, Metal–organic framework MIL-100(Fe) for the adsorption of malachite green from aqueous solution, J. Mater. Chem. 22 (2012) 7449.

[29] J. Shao, Z. Wan, H. Liu, H. Zheng, T. Gao, M. Shen, Q. Qu, H. Zheng, Metal organic frameworks-derived Co_3O_4 hollow dodecahedrons with controllable interiors as outstanding anodes for Li storage, J. Mater. Chem. A 2 (2014) 12194–12200.

[30] C.H. Hendon, D. Tiana, M. Fontecave, C. Sanchez, C. Sassoye, L. Rozes, Engineering the optical response of the titanium-mil-125 metal–organic framework through ligand functionalization, J. Am. Chem. Soc. 135 (2013) 10942–10945.

[31] K.Y.A. Lin, H. Yang, C. Petit, F.K. Hsu, Removing oil droplets from water using a copper-based metal organic frameworks, Chem. Eng. J. 249 (2014) 293–301.

[32] D. Sun, Y. Fu, W. Liu, L. Ye, D. Wang, L. Yang, X. Fu, Z. Li, Studies on photocatalytic co 2 reduction over nh 2 -uio-66(zr) and its derivatives: towards a better understanding of photocatalysis on metal-organic frameworks, Chem. A Eur. J. 19 (2013) 14279–14285.

[33] D.J. Tranchemontagne, J.R. Hunt, O.M. Yaghi, Room temperature synthesis of metal-organic frameworks: MOF-5, MOF-74, MOF-177, MOF-199, and IRMOF-0, Tetrahedron 64 (2008) 8553–8557.

[34] S. Pullen, H. Fei, A. Orthaber, S.M. Cohen, S. Ott, Enhanced photochemical hydrogen production by a molecular diiron catalyst incorporated into a metal–organic framework, J. Am. Chem. Soc. 135 (2013) 16997–17003.

[35] K.G.M. Laurier, F. Vermoortele, R. Ameloot, D.E. De Vos, J. Hofkens, M.B.J. Roe, Iron(III)-based metal – organic frameworks as visible light photocatalysts, J. Am. Chem. Soc. 100 (2013) 14488–14491.

[36] P. Kusgens, M. Rose, I. Senkovska, H. Fröde, A. Henschel, S. Siegle, S. Kaskel, Characterization of metal-organic frameworks by water adsorption, Microporous Mesoporous Mater. 120 (2009) 325–330.

[37] M. Ji, X. Lan, Z. Han, C. Hao, J. Qiu, Luminescent properties of metal – organic framework MOF-5: relativistic time-dependent density functional theory investigations, Inorg. Chem. 51 (2012) 12389–12394.

[38] M.S. Samuel, S. Suman, Venkateshkannan, E. Selvarajan, T. Mathimani, A. Pugazhendhi, Immobilization of Cu3(btc)2 on graphene oxide-chitosan hybrid composite for the adsorption and photocatalytic degradation of methylene blue, J. Photochem. Photobiol. B: Biol. 204 (2020), 111809, https://doi.org/10.1016/j.jphotobiol.2020.111809.

[39] S. Ayub, A.A. Mohammadi, M. Yousefi, F. Changani, Performance evaluation of agro-based adsorbents for the removal of cadmium from wastewater, Desalin. Water Treat. 142 (2019) 293–299.

[40] S. Sharifi, R. Nabizadeh, B. Akbarpour, A. Azari, H.R. Ghaffari, S. Nazmara, B. Mahmoudi, L. Shiri, M. Yousefi, Modeling and optimizing parameters affecting hexavalent chromium adsorption from aqueous solutions using Ti-XAD7 nanocomposite: RSM-CCD approach, kinetic, and isotherm studies, J. Environ. Heal. Sci. Eng. 17 (2019) 873–888.

[41] M. Heydari Moghaddam, R. Nabizadeh, M.H. Dehghani, B. Akbarpour, A. Azari, M. Yousefi, Performance investigation of zeolitic imidazolate framework – 8 (ZIF-8) in the removal of trichloroethylene from aqueous solutions, Microchem. J. 150 (2019), 104185.

[42] E.A. Abigail M, M. Samuel S, R. Chidambaram, Application of rice husk nanosorbents containing 2,4-dichlorophenoxyacetic acid herbicide to control weeds and reduce leaching from soil, J. Taiwan Inst. Chem. Eng. 63 (2016) 318–326.

[43] E.A.A. M, M.S. Samuel, R. Chidambaram, Optimization, equilibrium, kinetics and thermodynamic studies, J. Taiwan Inst. Chem. Eng. 49 (2014) 156–164.

[44] M.S. Samuel, E.A.A. M, R. Chidambaram, Biosorption of Cr(VI) by Ceratocystis paradoxa MSR2 Using isotherm modelling, kinetic study and optimization of batch parameters using response surface methodology, PLoS One 10 (2015) 1–23.

[45] M.S. Samuel, E.A. Abigail M, R. Chidambaram, Isotherm modelling, kinetic study and optimization of batch parameters using response surface methodology for effective removal of Cr(VI) using fungal biomass, PLoS One 10 (2015) 1–15.

[46] M.S. Samuel, S.S. Shah, J. Bhattacharya, K. Subramaniam, N.D. Pradeep Singh, Adsorption of Pb(II) from aqueous solution using a magnetic chitosan/graphene oxide composite and its toxicity studies, Int. J. Biol. Macromol. 115 (2018) 1142–1150, https://doi.org/10.1016/j.ijbiomac.2018.04.185.

[47] M.S. Samuel, V. Subramaniyan, J. Bhattacharya, R. Chidambaram, T. Qureshi, N. D. Pradeep Singh, Ultrasonic-assisted synthesis of graphene oxide – fungal hyphae: an efficient and reclaimable adsorbent for chromium(VI) removal from aqueous solution, Ultrason. Sonochem. 48 (2018) 412–417.

[48] M.S. Samuel, S.S. Shah, V. Subramaniyan, T. Qureshi, J. Bhattacharya, N. D. Pradeep, Singh, Preparation of graphene oxide/chitosan/ferrite nanocomposite

for chromium(VI) removal from aqueous solution, Int. J. Biol. Macromol. 119 (2018) 540–547.
[49] M.S. Samuel, J. Bhattacharya, S. Raj, N. Santhanam, H. Singh, N.D. Pradeep Singh, Efficient removal of chromium(VI) from aqueous solution using chitosan grafted graphene oxide (CS-GO) nanocomposite, Int. J. Biol. Macromol. 121 (2019) 285–292.
[50] M. Abigail, S. Melvin Samuel, C. Ramalingam, Addressing the environmental impacts of butachlor and the available remediation strategies: a systematic review, Int. J. Environ. Sci. Technol. 12 (2015) 4025–4036.
[51] E.A. Abigail M, M.S. Samuel, R. Chidambaram, Hexavalent chromium biosorption studies using Penicillium griseofulvum MSR1 a novel isolate from tannery effluent site: box-behnken optimization, equilibrium, kinetics and thermodynamic studies, J. Taiwan Inst. Chem. Eng. 49 (2015) 156–164.
[52] V.S. Kirankumar, N. Mayank, S. Sumathi, Photocatalytic performance of cerium doped copper aluminate nanoparticles under visible light irradiation, J. Taiwan Inst. Chem. Eng. 95 (2019) 602–615.
[53] L.Á. Alfonso Herrera, P.K. Camarillo Reyes, A.M. Huerta Flores, L.T. Martínez, J. M. Rivera Villanueva, BDC-Zn MOF sensitization by MO/MB adsorption for photocatalytic hydrogen evolution under solar light, Mater. Sci. Semicond. Process. 109 (2020), 104950.
[54] W. Jianmin, X. Teng, H. Wang, H. Ban, Characterizing the metal adsorption capability of a class F coal fly ash, Environ. Sci. Technol. 38 (2004) 6710–6715.
[55] D.R. Ledoux, G.E. Rottinghaus, A.J. Bermudez, M. Alonso-Debolt, Efficacy of a hydrated sodium calcium aluminosilicate to ameliorate the toxic effects of aflatoxin in broiler chicks, Poult. Sci. 78 (1999) 204–210.
[56] R. Sharma, S. Raghav, M. Nair, D. Kumar, Kinetics and adsorption studies of mercury and lead by ceria nanoparticles entrapped in tamarind powder, ACS Omega 3 (2018) 14606–14619.